An Investigation of the Fatigue Corrosion Behavior of Al 6063-T6 Alloy under Seawater Influence

R. Abdollahi[1], M. Hajisafari[1,*], A. Zare Bidaki[1]

[1]Department of Metallurgy and Materials Engineering, Yazd Branch, Islamic Azad University, Yazd, Iran.
Received: 3 June 2017 - Accepted: 5 August 2017

Abstract

The purpose of the present study was to investigate the fatigue behavior of Al-6063 alloy using standard rotating-bending test. Corrosion-fatigue test on similar samples was also performed at stress levels corresponding to fatigue test. The samples obtained from fatigue tests were considered as control samples and the results obtained from fatigue test in air were compared to the results obtained from corrosion-fatigue test in liquid seawater. Scanning Electron Microscopy (SEM) and Optical Microscopy (OM) were used to investigate the micro-structural features and crack characteristics of the specimens. The results obtained from fatigue and corrosion-fatigue test revealed that the presence of corrosion environment decreases the fatigue life. Additionally, microstructure studies on the fracture surface due to corrosion-fatigue revealed that initiation of fatigue crack starts from the depth of corrosion steps and proliferate towards the sample center simultaneous with the penetration of liquid into the crack. Moreover, the appearance, size and propagation way of fatigue crack in corrosion-fatigue test was completely different from the cracks created in a fatigue test. The fracture surface due to corrosion-fatigue test was also different from the fatigue fracture surface. Further studies on failure levels revealed that the ratio of region area due to fatigue to the region area due to final failure was strongly decreased in the corrosion-fatigue test.

Keywords: Corrosion Fatigue, Al 6063-T6 Alloys, Seawater, Crack Initiation, Striation lines.

1. Introduction

Aluminum alloys can be made by stir casting which is one of the economic ways for the production of metal composite. Stir casting is one of the simplest ways of producing aluminum composite [1]. Fatigue life is decreased by increasing factors' intensity in the environment and beginning cracking in grain boundary [2]. The interface of particles and grains in microscopic structures of materials plays an important role in the growth and formation of holes and cracks [3-4]. The primary defect size to predict fatigue life on the artifact and natural corroded alloy as well as statistical and experimental results confirms that the cracks start from the end of a hole where the pressure level reaches its critical value [5-6]. Fatigue failure is a phenomenon occurring due to the formation and growth of cracks. There is a comprehensive explanation about the microscopic behavior of these cracks and their proliferation [7]. Static shear pressures cause slips on the surfaces, which are coarse sliding stripes under cyclic conditions. The presence of sliding bands slightly takes place in this environment in which cracks start. The 6xxx series of aluminum alloys allocate a high volume of failure in aluminum products [8-10]. Due to its shaping capability, lightweight, corrosion resistance, good weld ability and very good mechanical properties, aluminum 6063 is used in automobile industry, aerospace, piping systems for irrigation, and electrical conductors [11]. The highest volume of aluminum products has been used in western countries (with global use of 23%). In the past five years, 80% of various industries have used this alloy. Above 46% of the aluminum alloy used for various applications has been used in plates or cold forms. High use of this alloy depends on the increase of mechanical properties such as elasticity and stiffness [12]. Mechanical properties of aluminum alloy are increased by refining its grain structure. Rolling out is a method to produce ultra-fast broadband materials (UFB) [13 ,14]. Employing solid liquid, before and after rolling, causes the increase of stiffness [15]. Annealing causes the formation of soft and semi-soft grains in cold-formed samples. Annealing aluminum through ECAP (Equal Channel Angular Pressing) method has been performed in various tensions. If crystallizing takes place with low tension, it is called non-permanent state, and if it takes place with high tension, it is called permanent state [16 ,17]. Alloys with high strength do not have a good fatigue life when they are subjected to fatigue loading [18]. The behavior of soft-grain alloy indicates that in fatigue with low cycle, the fatigue life of UFGs has been very shorter than that of typical grains. ECAP has been mostly employed in fatigue works [19]. All the 6063 alloys have been employed in the marine industry; therefore, its corrosion is highly important [20]. Now, if this alloy is employed in alternative loading conditions, fatigue phenomenon is discussed with corrosion [21]. Microstructure influences the mechanical properties, especially fatigue life.

[*]*Corresponding author*
Email address: hajisafari1001@iauyazd.ac.ir

Changing the microstructure of this alloy through applying thermal operations cycles leads to the improvement of its fatigue corrosion [22-24]. The most important thermal operations for these alloys are T4 and T6 operations. It is obvious that the presence of superficial cracks on a piece in a corrosive environment (seawater) can cause the decrease of fatigue corrosion of this alloy [25-27]. Higher corrosion resistance of Al 6063-T6 in comparison to the other group of metals results in decreasing corrosion products and higher working life of related structures and therefore reducing the environmental contamination. On the other hand, this material could be introduced as friendly environmental materials. Therefore, in the present study, fatigue and corrosion fatigue properties of Aluminum 6063 alloy were investigated using the standard Rotating-Bending method, and the obtained results from fatigue test were compared to data achieved by corrosion fatigue test conducted on similar samples using the same stress levels.

2. Materials and Methods

In order to prepare the samples, Aluminum 6063-T6 alloy rod with nominal diameter of 10 mm was used. Table 1. given the results obtained for determining chemical combinations of Al 6063-T6 sample. The data presented in this table is in accordance with ASTM B221 standard [28]. The tensile properties and hardness of samples, which were investigated by the uniaxial tensile testing method (GOTECH), and micro hardness test (Future-Tech FM-700) respectively, are listed in Table 2. Al 6063-T6 rods were machined using a CNC lathe in accordance with ASTM-E466 standard [29], so that in order to minimize the surface residual stress throughout the machining procedure, a very strong control was performed on machining procedure concurrent with sample cooling. In the next step, to obtain desired specimens gauge area surface quality, the polishing process was performed on the previously mentioned surface of all samples using emery papers No. 1000, 1500, 2000, 2500 and 3000. However, the polishing steps were followed by using polishing paste and finally cotton to avoid notch effects and surface grooves. The high cycle fatigue test was carried out using SANTAM rotating –bending fatigue testing machine (SANTAM, Ltd. IRAN) at different stress amplitudes. Similarly, corrosion fatigue tests inside seawater were accomplished using MSA 2013 corrosion fatigue testing machine. In both tests, a sinusoidal cyclic waveform with cycling frequency of 5.0 Hz and a load ratio R= -1 were adopted so that for each stress level three identical samples were tested. In addition, in corrosion fatigue tests, the solution temperature was adjusted to the range of 25±1˚C, which was continuously monitored with the accuracy of 0.1˚C throughout the tests. Furthermore, in order to minimize the chance of galvanic corrosion between the sample and sample holders, both ends of selected sample were insulated with inelastic insulator prior to start of each test. Moreover, specimens were exposed to the liquid environment 2 hours before the start of loading. The stress levels of cyclic loading, in both fatigue and corrosion fatigue tests, started at 150 MPa and finished at approximately 75 MPa. Specimens fracture surfaces were examined using field emission scanning electron microscopy (FESEM, MIRA3 TESCAN) and scanning electron microscopy (ESEM, VEGA TESCAN) equipped with energy-dispersive X-ray spectroscopy (EDS) and backscattered electron detector. Additionally, MIP (Micro-structural Image Processor) software was used for SEM micrographs analysis.

3. Results and Discussion

Fig. 1. shows an optical microscopic image from the surface of the as-received samples. As it can be seen from this figure, the microstructure of the alloy consists of the two phases, α and β.

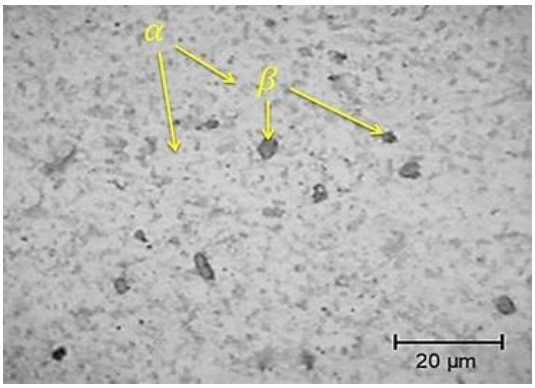

Fig. 1. The optical microscope of the as-received sample.

Table 1. Chemical composition of Al 6063-T6 alloy (wt. %) [28].

Al	Si	Fe	Cu	Mn	Mg	Cr
Residual	0.350	0.080	0.030	0.010	0.500	0.002
Ca	**Pb**	**V**	**Na**	**Bi**	**Co**	**Cd**
0.002	0.003	0.010	0.002	0.010	0.003	0.005

Table 2. Mechanical properties of Al 6063-T6 alloy.

Tensile Strength (MPa)	Yield Strength (MPa)	Elongation (%)	Hardness (Vickers)	Hardness α (Vickers)	Hardness β (Vickers)
211	189	12%	95.77	74	85

Fig. 2. shows SEM images from the cross section of the samples. As it can be seen in this figure, the phase β has been evenly distributed in the microstructure. This distribution can be due to thermal operations of Ts in which, after heating up to the temperature of 150 °C, the alloy is cooled in air. During cooling, Mg_2Si particle forms. Increasing the Si content of the alloy will lead to the fine particles of Mg_2Si which can improve the age hardening properties of the alloy.

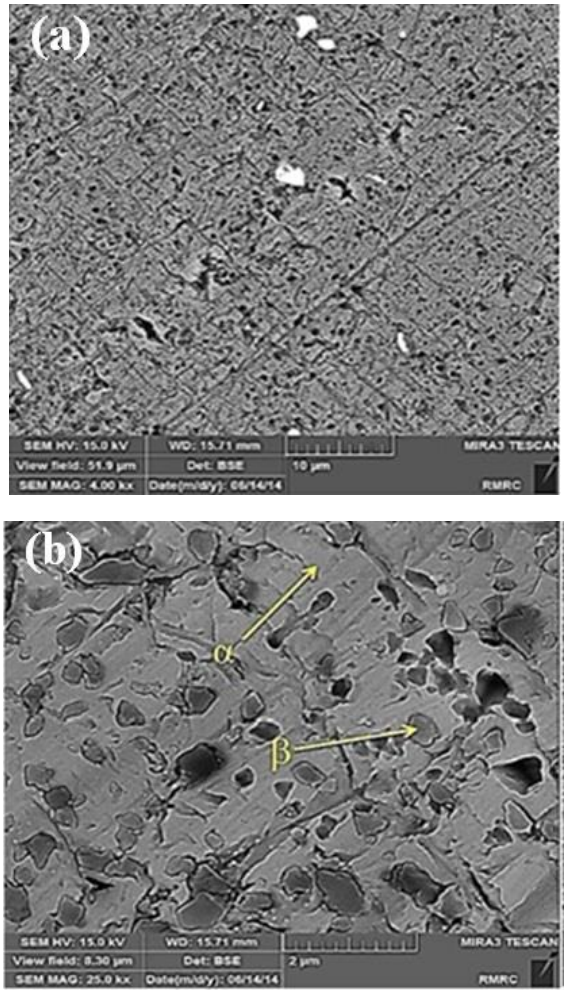

Fig. 2. FESEM images from the cross section of samples before fatigue test at different magnifications.

Table 3. Energy-dispersive X-ray spectroscopy (EDS) results of the phases α and β from Fig. 2b.

Phase	Al (wt. %)	Mg (wt. %)	Si (wt. %)
α	98.74	1.00	0.26
β	98.62	0.98	0.40

As determined in Table 3., the magnitude of Mg is almost twice greater than Si magnitude in the phase. The hardness of the phase β is probably higher than phase α. To obtain the hardness level of the alloy employed in the tests, micro hardness test was performed on the fatigued sample (Fig. 3.). Given the approximate evenness of the hardness level in line with the diameter, this fact can be a reason for the evenness dispersion of phase β in field phase α. The recoded optical microscopic images of the sample surface before fatigue test (Fig. 1.) evidently suggest this fact.

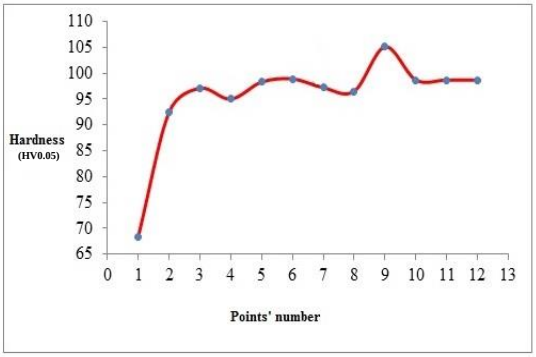

Fig. 3. Micro hardness profile of the fatigued surface.

Fig. 4. depicts the S-N curve (stress-the number of cycles to failure) related to the Al-6063 alloy in the air and inside seawater. As the figure shows, the alloy's fatigue strength at the room temperature is 75 MPa and its fatigue life is 7.3×10^6. As it can be seen, the last stress level (in which the piece has suffered from a failure) is 75 MPa and after 7.3×10^6, it has been suffered failure. However, performing fatigue test on another sample of the alloy, the cycle has suffered failure in 70 MPA stress level and after 13×10^6, indicating the ultra-life of the alloy. Furthermore, comparing the two curves reveals that this alloy shows a different behavior in the seawater. In other words, subjecting the samples to corrosion-fatigue test, fatigue strength and fatigue life decrease at corresponding stress levels. Corrosion fatigue in aqueous media is an electrochemical behavior. The presence of a corrosive environment during loading fatigue leads to corrosion pits. Fractures are initiated either by pitting or persistent slip bands. In this alloy, pitting will often be the most damaging type of corrosion, degrading performance by increasing the crack initiation and crack-growth rate more than any other kind of corrosion. Notably, to compare fatigue and corrosion-fatigue tests, the selected stress levels and applied stress levels have been considered identical in the fatigue test.

Fig. 5. presents the fracture surface of the sample failed after 7.3×10^6 cycle. As it can be seen, about 80% of the failure is due to fatigue phenomenon and the remaining 20% is due to soft failure in the final stage. Furthermore, in corrosion fatigue, the failure area due to fatigue has been strongly decreased relative to fatigue test samples (compared Fig. 5a and 5b) and the area with fragile crack has been increased compared to the corresponding area in a fatigue test.

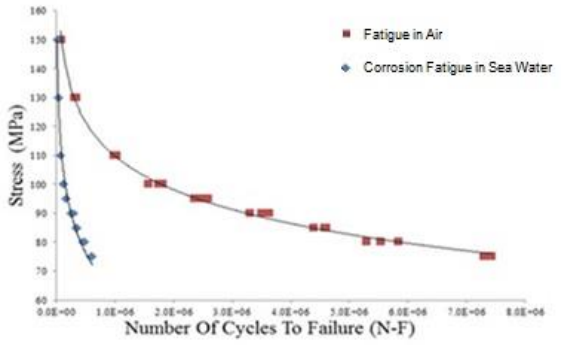

Fig. 4. S-N curves of aluminum samples in the presence of air and in Seawater.

Higher magnification of Fig. 5. was exhibited in Fig. 6. As seen, unlike ductile fracture mode of air fatigued specimen (Fig. 6a), the mode of fracture of seawater fatigued specimen was semi-ductile fracture (Fig. 6b). Presence of dimples in the fracture surface of air-fatigued specimens indicated the ductile fracture mode, while faceted zone between dimple areas in the fracture surface of seawater-fatigued specimens indicated the semi-ductile fracture.

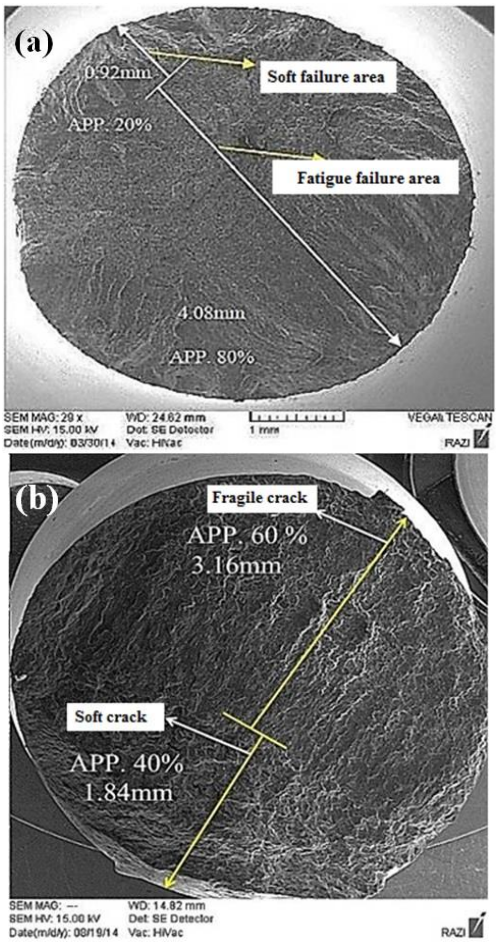

Fig. 5. SEM fractography of samples. (a) Air-fatigued surface, (b) corrosion fatigued surface in a seawater environment.

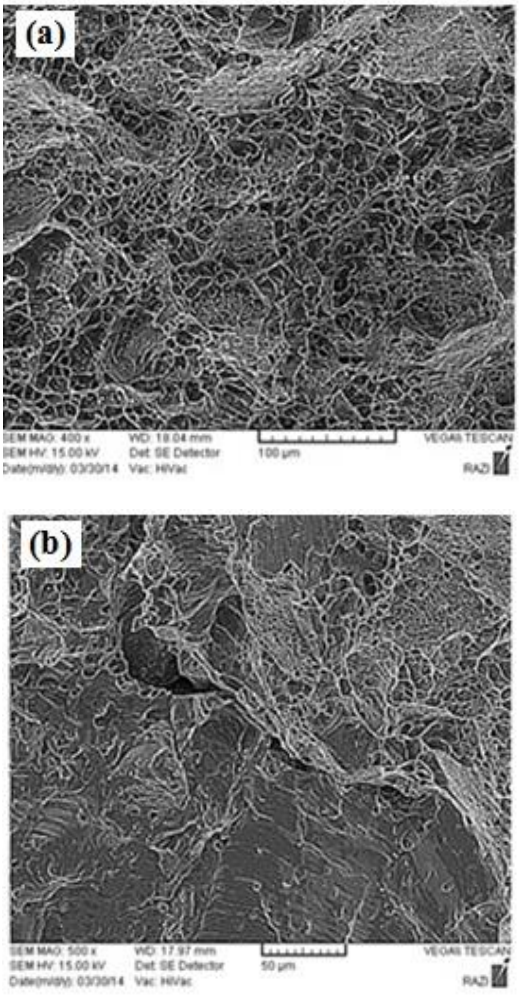

Fig. 6. SEM images of the fatigue fracture surface of the Al-6063 alloy tested in (a) air environment, (b) seawater environment.

Fig. 7. shows SEM images of the fatigue failure area (Fig. 5a). As the figure presents, striation lines due to the applied stress cycles can be observed during fatigue loading in this area.

As shown in Fig. 8a, edge crack (a_1) and internal crack (a_2) can be seen on the fracture surface. Fig. 8b shows the crack a_1 in a higher magnification. It can be seen that the crack initiated from the sample surface and continued towards the center. Ups and downs created on the surface are due to the cyclic loadings, and fatigue cracks start from these ups and downs.

The superficial crack initiations occur at the place of superficial defects (i.e., superficial unevenness, superficial stress sources, and changes in residual superficial stress or the change of fatigue strength). Considering the fact that the tested samples have been totally subjected to polishing process, unevenness in surface cannot cause crack initiation. Mg_2Si sediment is created in thermal operations in which the rate of chilling is below zero centigrade.

Therefore, fatigue crack initiation due to hard Mg_2Si sediment is improbable.

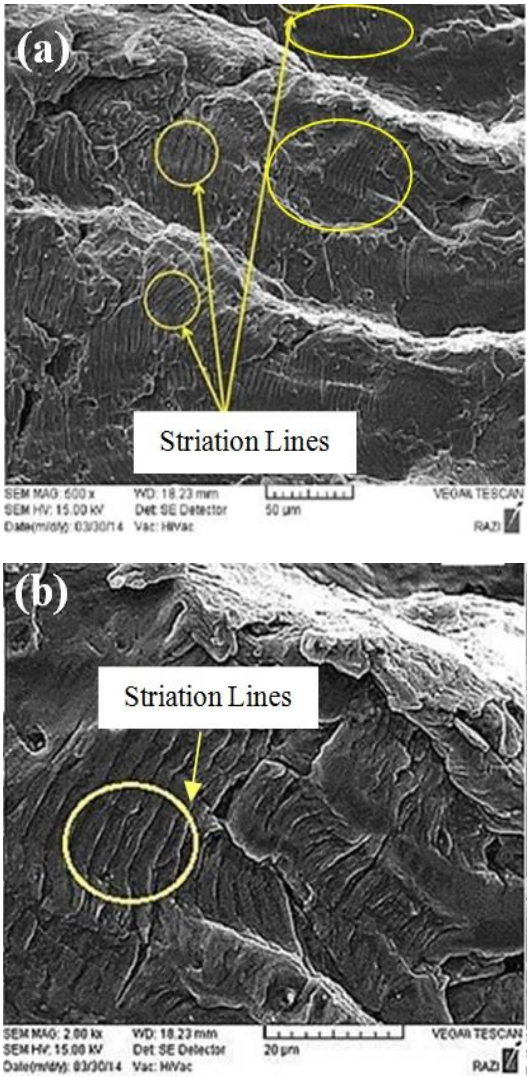

Fig. 7. Striation lines in the fatigue fracture surface at different magnification.

Additionally, since the maximum care has been applied in chilling and abrasive flow machining during the machine working process, the presence of residual stress of the surface cannot either be the cause of crack initiation. Accordingly, since initiation and crack growth path have been thoroughly placed in the phase of α and the path is deviated by encountering the phase β, initiation and crack growth way as well as fatigue crack propagation in this alloy can be attributed to the strength level of the existing phases. In other words, crack changes its path when it encounters a phase with higher strength and continues to proceed in the softer phase. Also, the presence of ups and downs created due to cyclic loading can be another reason for the creation of the sample edges crack (Fig. 8c). Hence, crack starts from the depth of down and deviates from its path by keeping on crack development in the phase of α during several stages after encountering the hard β phase (Fig. 9a and b).

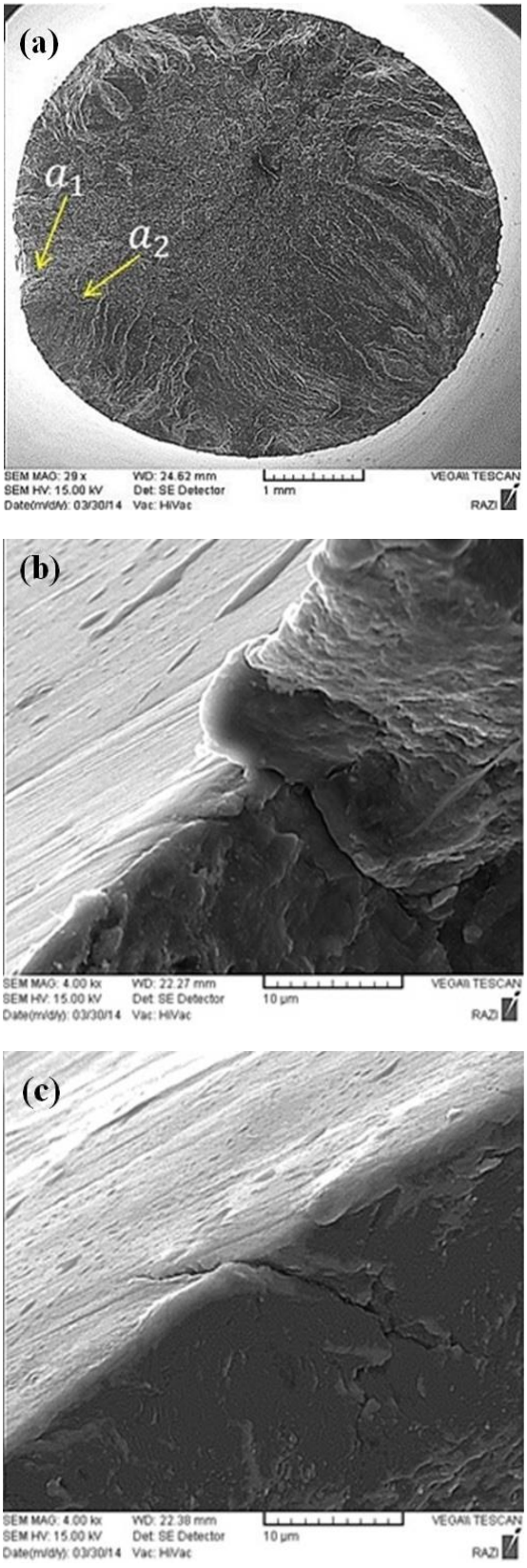

Fig. 8. SEM image of the micro-cracks in the fatigue surface. (a) macro-graph, (b) and (c) illustrate surface crack that was determined via a_1 arrow.

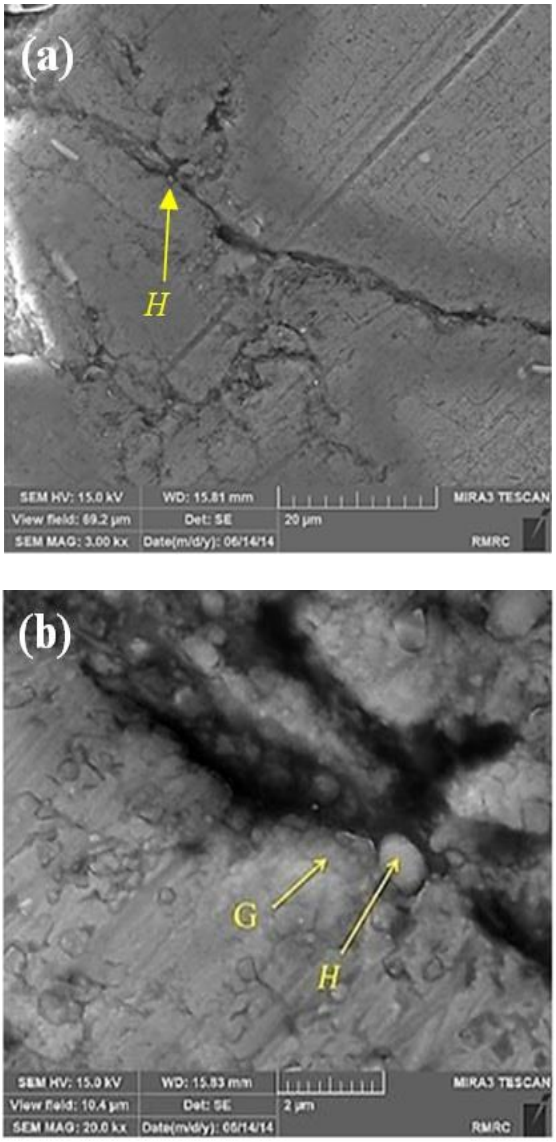

Fig. 9. FESEM images of initiation and propagation of crack a_1 in Fig. 8. at different magnification.

Table 4. given the chemical analysis result around the crack in two phases of α and β of Fig. 9b. Fig. 10. also presents EDS of the sample surface in the mentioned phases. As expected, in terms of constituents, the phase α has a higher aluminum content than the phase β and the amount of Mg and Si is less in the phase α. Therefore, the higher strength level of the phase β can be due to higher amount of Mg and Si in this phase.

Table 4. The analysis results of chemical combination of the sample's surface in the phases α and β.

Phase	Al (wt. %)	Mg (wt. %)	Si (wt. %)
α	99.33	0.22	0.45
β	98.38	0.54	1.08

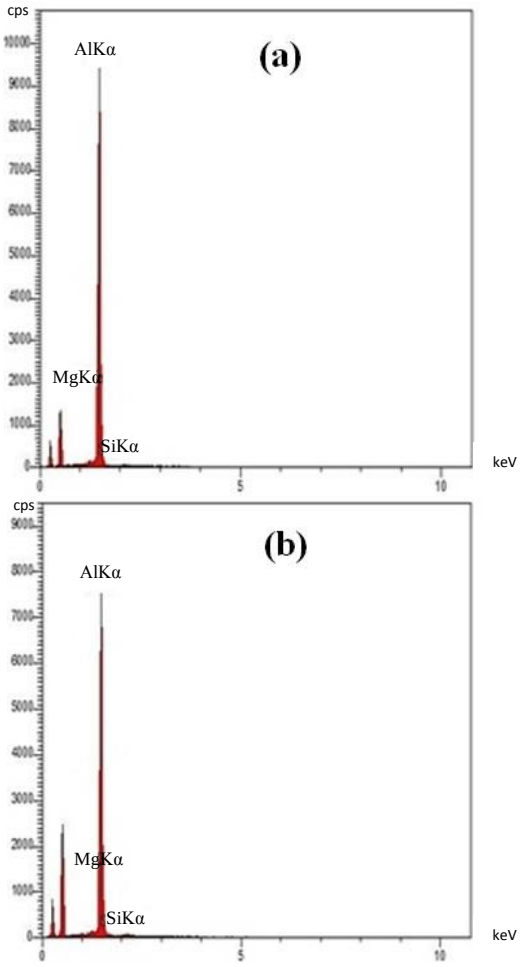

Fig. 10. EDS results of different phases in Fig. 9b, (a) α phase, (b) β phase.

Further studies on the crack propagation way indicate that in some cases, there are branches in the crack path. Fig. 11. shows an instance of such behavior in which the crack deviates from its path when encountering the phase β.

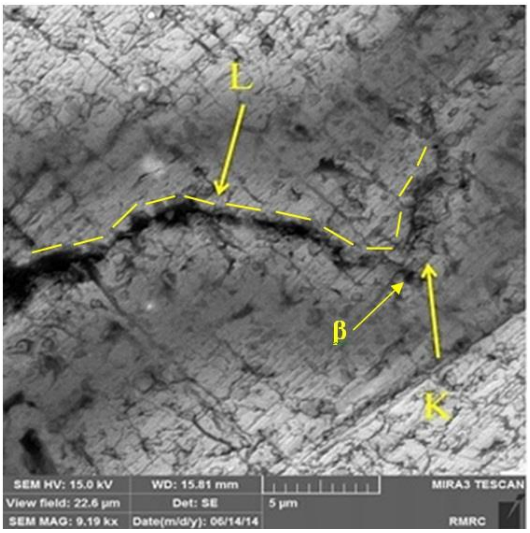

Fig. 11. The fatigue behavior of crack encountering the β phase. K and L indicate the crack deviation.

Fig. 12a shows that the crack a_2 is an internal crack, i.e. its initiation occurs within the sample (point M) and its propagation continues within the sample in a limited way. Similar to the crack a_1, this crack experiences splits and branches in its propagation path when encountering the second phase. As shown, in the Al-6063 alloy, an internal crack has been observed at the failure level of a sample, which endured 4572917 stress cycles. These cracks can be due to the presence of hard phase of β at the crack place. Fig. 12b shows the chemical combination analysis of the crack initiation place (point M). More investigation that is precise reveals that the crack initiates from the hard phase of β. The chemical analysis from point M is determined in Table 5.

Table 5. Chemical combinations analysis from point M.

Existing elements (wt. %)		
Al	**Mg**	**Si**
98.88	0.72	0.4

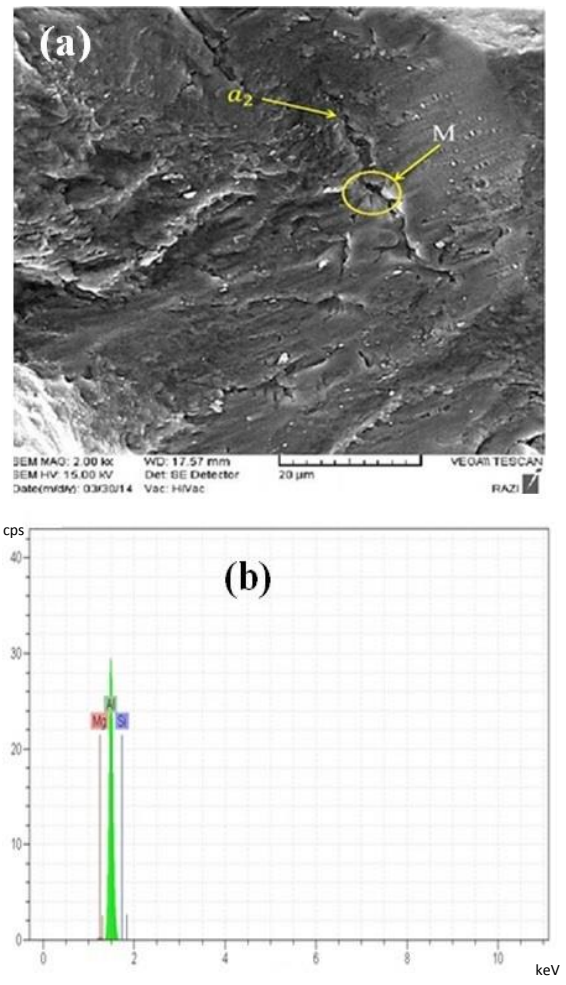

Fig. 12. (a) SEM image of initiation and propagation path of crack a_2, (b) EDS of point M.

Fig. 13. shows SEM images of failure level in corrosion-fatigue failure area. The figure also shows the striation lines created due to cyclic loading in this area.

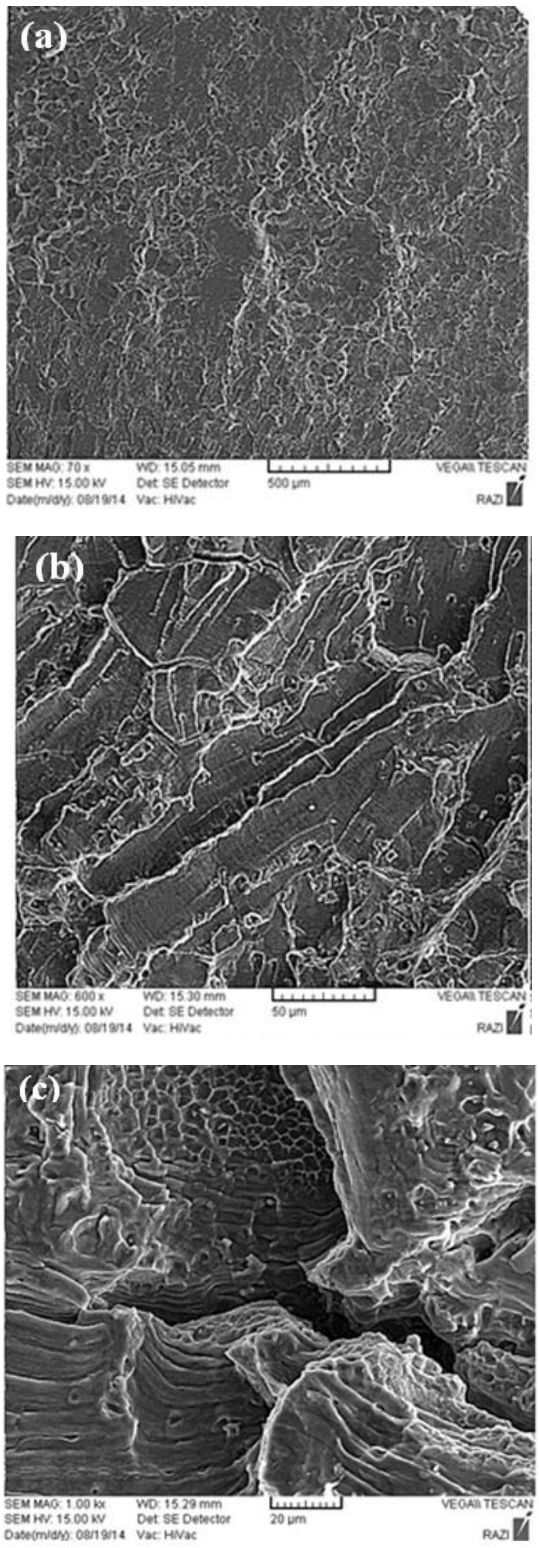

Fig. 13. SEM fractography of corrosion fatigued fracture surface at different magnifications.

In Figs. 14a and b, there are cracks, which are created due to corrosion-fatigue test. These cracks are softer and scattered on the fracture surface. Moreover, as shown in Fig. 14c , corrosion products can be clearly seen on the fracture surface in a scattered manner. They are all on the surface of the sample.

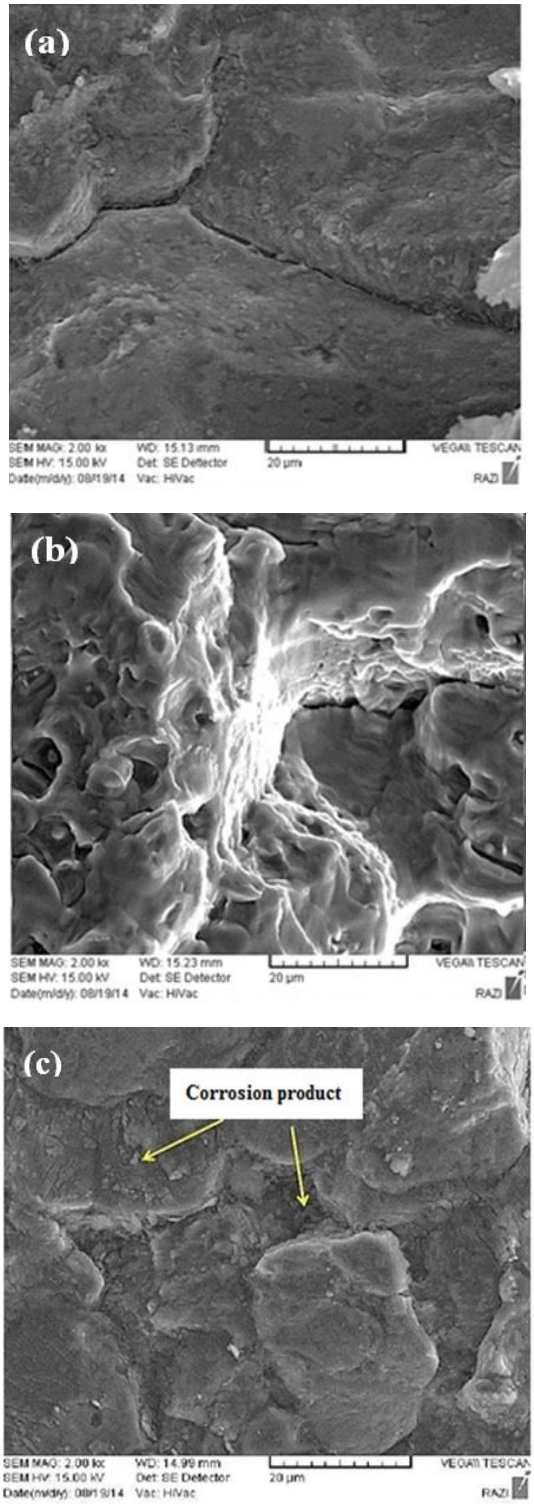

Fig. 14. SEM fractography of initiation of an internal crack on the corrosion fatigued fracture surface (a and b) and corrosion product around internal crack.

Fig. 15. shows the images of the fracture surface of the samples in air and inside seawater. As it can be seen, striation lines distance and stair-like unevenness in the sample under corrosion-fatigue test are less than those in the samples fractured due to fatigue in the air. This is attributed to the presence of an aggressive environment surrounding the fracture surface throughout the cyclic loading. Occurrence of corrosion phenomenon on the fracture surface caused surface grooves height reduction, and as a result, the distance between two vicinal peaks decreased.

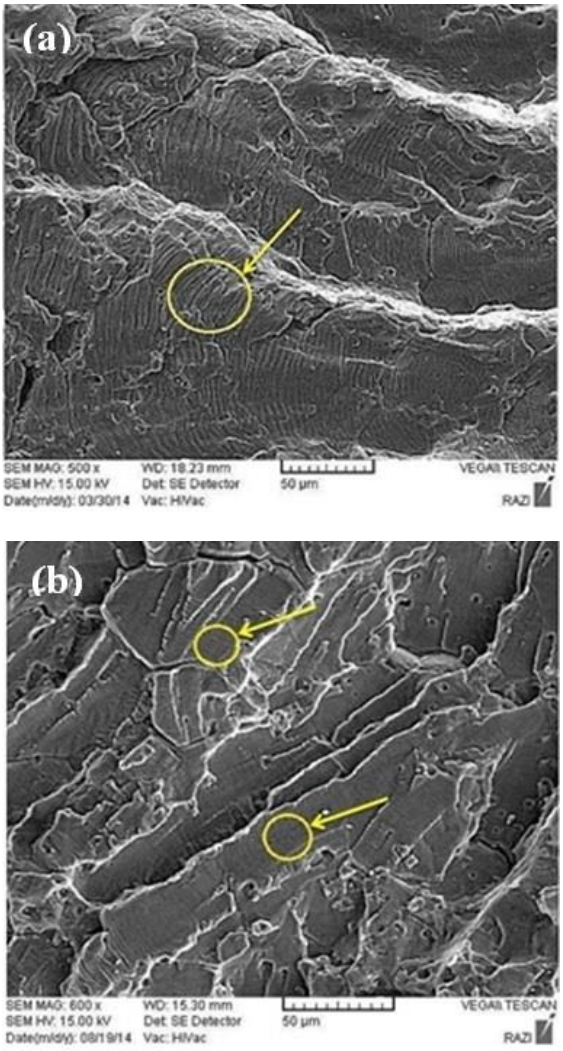

Fig. 15. Comparison of striation lines in fatigued samples. (a) in the air and (b) in seawater.

SEM studies of the fractured surfaces indicated the contribution of corrosion on the occurring of fracture, i.e. presence of corrosive products on the fracture surfaces illustrated this contribution (Fig. 16.).

According to the Fig. 16. and the results obtained from chemical composition determination test (Table 6 and 7), these materials can be considered as corrosion products.

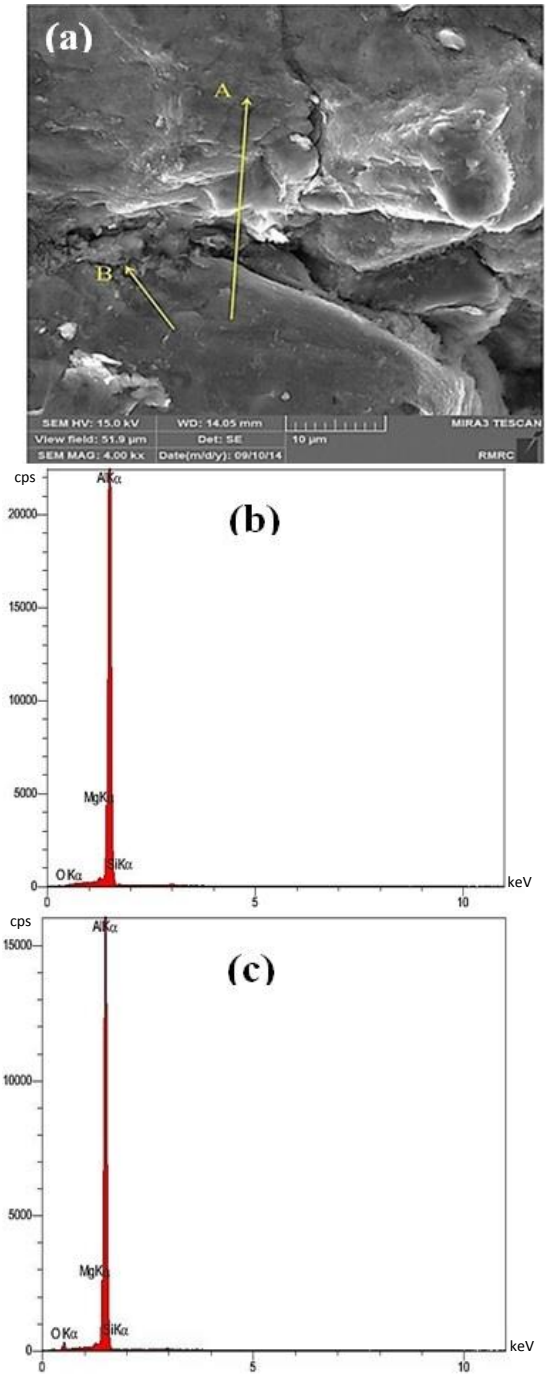

Fig. 16. (a) SEM images of the corrosion fatigued fracture surface, (b) EDS of point A, (c) EDS of point B.

Table 6. Chemical composition test results related to point A (Fig. 16a)

Existing elements (wt. %)			
Al	**Mg**	**Si**	**O_2**
98.17	0.94	0.21	0.68

Table 7. Chemical composition test results related to point B (Fig. 16a)

Existing elements (wt. %)			
Al	**Mg**	**Si**	**O_2**
90.55	0.92	0.22	8.31

4. Conclusions

1. The studied Al-6063 alloy's fatigue strength at room temperature was 75 MPa and its fatigue life was 7.3×10^6. By subjecting the samples to seawater and applying a cyclic load to them, fatigue strength was removed and its fatigue life was 5.7×10^5 in the stress of 75 MPa.
2. The incidence of fatigue phenomenon had a significant effect on the strength of the alloy under the test. The life of the similar samples significantly decreased under identical loading conditions in corrosion-fatigue test.
3. The presence of higher magnitudes of Mg and Si elements in the phase β increased the strength of that phase.
4. Investigating the microstructure of the studied alloy revealed that this alloy has the two phases of α (field phase) and β and initiation of fatigue crack takes place in the phase α.
5. Fatigue crack propagation occurs from the sample edge and in the phase α. In addition, the crack is encountering the harder phase of β causes deviation from propagation path and splits in the crack.
6. The apparent shape of fatigue cracks is very different on the sample's fracture surface from the corrosion-fatigue cracks in terms of size and propagation behaviour of the crack.
7. The penetration of the seawater into the span of the fatigue crack causes changes in the apparent shape of fracture surfaces.
8. Corrosive environment increases brittle fracture percentage (~20%) during the application of cyclic loading.
9. The decrease of the fatigue strength of the Al-6063 alloy due to corrosion caused the decrease of stair surface due to fatigue**,** and the accumulation of corrosion beside these stairs stopped the crack growth as well as the initiation and propagation of the crack from the next stair.

References

[1] N. V. Murthy, A. P. Reddy, N. Selvaraj and C. S. P. Rao, Int. J. Mech. Eng., 4(2015), 29.
[2] M. R. Bayumjt, Eng. Frac. Mech., 45(1993), 297.
[3] J. Kimberli, and D. W. Hoeppner. Int. J. Fatigue., 31 (2009), 686.
[4] A. G. M. Domínguez, J. L. Á. Ambriz and E. C. Calderón, Eng. Frac. Mech., 93(2012), 119.
[5] J. Kimberli and D. W. Hoeppner, Int. J. Fatigue., 31 (2009), 686.
[6] Q. Y. Wang, N. Kawagoishi and Q. Chen, Scripta Mater., 49(2003), 711.
[7] R. A., S. A. Abdul-Wahab Siddiqui, and T. Pervez, Mater. Des., 29(2008), 70.
[8] W. Onteiro, I. Espósito, R. Ferrari and S. Buso, Mater. Sci. Appl., 30(2011), 89.

[9] S. K. Panigrahi and R. Jayaganthan, Mater. Sci. Eng. A, 492(2008), 300.
[10] S. K. Panigrahi and R. Jayaganthan. J. Mater. Sci., 45(2010), 5624.
[11] O. I. Oluwole and J. A. Omotoyinbo, Mater. Res., 13(2010), 125.
[12] W. Klöpffer, Int. J. Life Cycle Assess, 17 (2012), 1087.
[13] S. K. Panigrahi, R. Jayaganthan and V. Chawla, Mater. Lett., 62(2008), 2626.
[14] T. S. Shih, Y. Hwa-Sheng and H. Wen-Nong, Metals, 6(2016), 51.
[15] H. Maruff, P. Nageswara Rao, D. Singh, R. Jayaganthan and S. Singh, Proced. Eng., 75(2014), 129.
[16] C. Joon-Yeon and A. Shan, Mater. Sci. Eng. A, 347(2003), 165.
[17] D. R. Fang, Z. F. Zhang, S. D. Wu, C. X. Huang, H. Zhang, N. Q. Zhao and J. J. Li., Mater. Sci. Eng. A, 426(2006), 305.
[18] M. D. Sangid, Int. J. Fatigue., 57(2013), 58.
[19] A. Vinogradov and H. Satoshi, Mater. Trans., 42(2001), 74.
[20] S. O. Adeosun, O. I. Sekunowo, S. A. Balogun, and V. D. Obiekea. Int. J. Corr., 2012(2012), 1.
[21] S. J. Price and B. F. Rita, Coat., 7(2017), 25.
[22] F. Walther, Mater. Test., 56(2014), 519.
[23] C. J. Villalobos-Gutiérrez, G. E. Gedler-Chacón, J. G. La Barbera-Sosa, A. Piñeiro, M. H. Staia, J. Lesage, D. Chicot, G. Mesmacque, and E. S. Puchi-Cabrera. Surf. Coat. Technol., 202(2008), 4572.
[24] Y.Q. Zheng, Z. Zhang, Fire Mater. 40(2016), 141.
[25] Z. Ling, Y.Li, Z.Luo, S. Ao, Z. Yin, Y. Gu, and Q. Chen, Int. J. Adv. Manuf. Technol. (2017), 1.
[26] N. Toric, J. Brnic, I. Boko, M. Brcic, I. W. Burgess and I. Uzelac, Metals, 7(2017), 1.
[27] K.J. Fann, and C.C. Chen, Appl. Sci., 7(2017), 372.
[28] ASTM B221, Standard Specification for Aluminum and Aluminum-Alloy Extruded Bars, Rods, Wire Profiles, and Tube,
[29] ASTM E466, Standard Practice for Conducting Force Controlled Constant Amplitude Axial Fatigue Tests of Metallic Materials. 0301: Metals - Mechanical Testing; Elevated and Low-Temperature Tests; Metallography. West Conshohocken, (2015).